Spin observables for polarized proton scattering from polarized ^{3}He

R. H. Landau, M. Sagen, and G. He
Physics Department, Oregon State University, Corvallis, Oregon 97331
(Received 5 May 1989)

Polarization observables for the scattering of two spin-$\frac{1}{2}$ particles are organized into different classes based on the difficulty of their measurement. The large or significantly varying ones are noted. A microscopic, momentum space optical potential is used to predict all polarization observables for 250–650 MeV proton scattering from the ^{3}He nucleus, and the observables are presented in three-dimensional plots.

I. INTRODUCTION

From the earliest days of nuclear physics it was recognized that the high spin dependence of the nucleon-nucleon force makes it possible to use proton-nucleus scattering to study the spin structure of nuclei.[1] Experimental advances—some quite recent[2]—permitting the scattering of polarized nucleons from polarized targets promise to provide further and more accurate determination of the distribution of spin within nuclei. This appears particularly promising in scattering from the spin-$\frac{1}{2}$ ^{3}He nucleus since, to a good approximation, the spin of the nucleus resides on $\frac{1}{3}$ of its nucleons (the two proton's spins are essentially paired to zero). In contrast, the spin-$\frac{1}{2}$ ^{13}C nucleus—to a good approximation—has its spin residing on $\frac{1}{13}$ of its nucleons, and so spin effects are proportionately less important.

The spin $\frac{1}{2}\times\frac{1}{2}$ phenomenology appropriate to the scattering of nucleons from ^{3}He is much like that of the two-nucleon problem: At each energy and angle six complex amplitudes describe the results of all possible experiments.[3,4] Understanding this phenomenology with its various tensor observables is neither simple nor universal—as witnessed by the extensive yet highly specialized literature on the subject. While it is unlikely that all of the 36 independent experiments possible for two spin-$\frac{1}{2}$ particles will be performed, the simpler ones—and some more complex ones which promise to yield important physics—are already being planned.

In this paper we provide predictions for the p-^{3}He elastic scattering observables possible with a polarized proton beam of energy 250–650 MeV and a polarized target. We tabulate the observables by degree of difficulty (the number of initial and final polarizations required), and find that few observables require the very difficult measurement of the recoiling target's polarization.

The actual predicted values for the observables arise from a microscopic, momentum-space optical potential[5,6] Eq. (1) containing the $\frac{1}{2}\times\frac{1}{2}$ spin dependence of nucleon-nucleon (NN) and nucleon-trinucleon scattering, nuclear form factors derived from three-body calculations of ^{3}He and ^{3}H, proper off-energy-shell kinematics, no small-angle approximations, and an off-energy-shell, NN T matrices based on modern phase shifts[8,9] and potentials.[10] While this basic theory can be improved by including effects such as many-body antisymmetrization, NN correlations, singlet-triplet mixing, Dirac-like relativity, and quark currents, no theory of that sort yet exists. Previous calculations with the present model[5,6] have provided gross understanding of low- and high-momentum-transfer differential cross sections.

II. THEORY

A. First-order optical potential

We describe p-^{3}He scattering with the momentum-space optical potential

$$
\begin{aligned}
U(\mathbf{k}',\mathbf{k};E)\simeq N\{&(t^{pn}_{a+b}+t^{pn}_{e}\sigma^{p}\cdot\hat{n})\rho^{n}_{mt}(q)+[t^{pn}_{a-b}\sigma^{p}\cdot\hat{n}\,\sigma^{A}\cdot\hat{n}+t^{pn}_{e}\sigma^{A}\cdot\hat{n}+t^{pn}_{c+d}\sigma^{p}\cdot\hat{m}\,\sigma^{A}\cdot\hat{m}\\
&+t^{pn}_{c-d}\sigma^{p}\cdot\hat{l}\,\sigma^{A}\cdot\hat{l}+t^{pn}_{c+d}(\sigma^{p}\cdot\hat{m}\,\sigma^{A}\cdot\hat{l}+\sigma^{p}\cdot\hat{l}\,\sigma^{A}\cdot\hat{m})]\rho^{n}_{sp}(q)\}\\
+Z\{&(t^{pp}_{a+b}+t^{pp}_{e}\sigma^{p}\cdot\hat{n})\rho^{p}_{mt}(q)+[t^{pp}_{a-b}\sigma^{p}\cdot\hat{n}\,\sigma^{A}\cdot\hat{n}+t^{pp}_{e}\sigma^{A}\cdot\hat{n}+t^{pp}_{c+d}\sigma^{p}\cdot\hat{m}\,\sigma^{A}\cdot\hat{m}\\
&+t^{pp}_{c-d}\sigma^{p}\cdot\hat{l}\,\sigma^{A}\cdot\hat{l}+t^{pp}_{c+d}\sigma^{p}\cdot\hat{m}\,\sigma^{A}\cdot\hat{l}+\sigma^{p}\cdot\hat{l}\,\sigma^{A}\cdot\hat{m})]\rho^{p}_{sp}(q)\}\ ,
\end{aligned}
\tag{1}
$$

where the superscripts A and p refer to the target nucleus and projectile proton, respectively. Here $\mathbf{k}$ and $\mathbf{k}'$ are the incident and scattered proton momenta in the p-^{3}He center of momentum (COM) frame, and $\mathbf{q}$ is the momentum transfer

$$\mathbf{q}=\mathbf{k}'-\mathbf{k},\quad q^2=k^2+k'^2-2kk'\cos\theta_{kk'}\ . \tag{2}$$

The unit vectors $\hat{n}$, $\hat{l}$, and $\hat{m}$ are

$$\hat{n}=\frac{\mathbf{k}\times\mathbf{k}'}{|\mathbf{k}\times\mathbf{k}'|},\quad \hat{m}=\frac{\mathbf{k}-\mathbf{k}'}{|\mathbf{k}-\mathbf{k}'|},\quad \hat{l}=\frac{\mathbf{k}+\mathbf{k}'}{|\mathbf{k}+\mathbf{k}'|}\ . \tag{3}$$

As indicated in Fig. 1, $\hat{n}$ is *normal* to the scattering plane (the plane defined by $\mathbf{k}$ and $\mathbf{k}'$), $\hat{l}$ is *in* the scattering plane and *longitudinal,* and $\hat{m}\equiv\hat{q}$ is in the scattering plane and in the *momentum*-transfer direction (*sideways* to the initial beam). The vectors $\hat{l}$ and $\hat{m}$ are orthogonal for on-shell ($k'=k$) scattering.

The ρ's in (1) are form factors describing the matter and spin distributions for neutrons and protons within the ^{3}He nucleus, and arise when we evaluate the expectation values of a bound nucleon's spin-dependent T matrix between initial and final nuclear states.[6] Consequently, the nuclear spin operator is introduced into (1) via the expectation value of a *bound* nucleon's spin being proportional to the nucleus's spin,

$$\langle\Psi^f_A|\sigma^p|\Psi^i_A\rangle=\sigma^A\rho^p_{sp}(q)\ , \tag{4}$$

$$\langle\Psi^f_A|\sigma^n|\Psi^i_A\rangle=\sigma^A\rho^n_{sp}(q) \tag{5}$$

with the proportionality constants just the appropriate nuclear spin form factors $\rho^n_{sp}(q)$ and $\rho^p_{sp}(q)$.

The t's in (1) are parts of the off-energy-shell NN T matrix. They are evaluated in the p-^{3}He COM and are functions of the momenta $\mathbf{k}'$ and $\mathbf{k}$ and subenergy $\omega[E]$. The full pN and p-^{3}He T matrix has the spin-space structure

$$\begin{aligned}T=\tfrac{1}{2}[&(a+b)+(a-b)\sigma_p\cdot\hat{n}\sigma_2\cdot\hat{n}+(c+d)\sigma_p\cdot\hat{m}\sigma_2\cdot\hat{m}\\&+(c-d)\sigma_p\cdot\hat{l}\sigma_2\cdot\hat{l}+e(\sigma_p+\sigma_2)\cdot\hat{n}\\&+f(\sigma_p-\sigma_2)\cdot\hat{n}]\ ,\end{aligned} \tag{6}$$

where "2" can be either the other nucleon or the nucleus, respectively.

While the f part of the NN T matrix vanishes if the generalized exclusion principle (including isospin) is invoked, that symmetry argument does not require the corresponding term in the p-^{3}He T matrix to vanish since the target and projectile are not identical. In fact, while not manifested from the form of the optical potential (1), the spin-orbit (t_e) terms in it are equivalent to *both* e- and f-like terms in the p-^{3}He potential. To see this,[7] we separate out the t_e terms in the potential (1) (keeping in mind that the resulting T matrix will have the same structure)

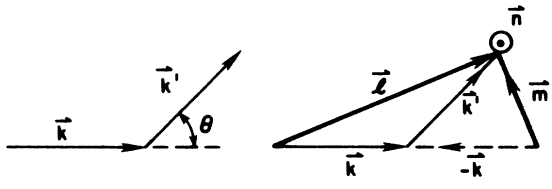

FIG. 1. The incident and scattered proton momenta ($\mathbf{k},\mathbf{k}'$) and the three unit vectors defined by Eq. (3).

$$\begin{aligned}U^{SO}=&Nt^{pn}_e\sigma^A\cdot\hat{n}\rho^n_{sp}+Nt^{pn}_e\sigma^p\cdot\hat{n}\rho^n_{mt}\\&+Zt^{pp}_e\sigma^A\cdot\hat{n}\rho^p_{sp}+Zt^{pp}_e\sigma^p\cdot\hat{n}\rho^p_{mt}\ .\end{aligned} \tag{7}$$

To transform this into the form of (6), we rewrite it in terms of sums and differences of σ^A and σ^p:

$$U^{SO}=U_e+U_f\ , \tag{8}$$

$$U_e=\tfrac{1}{2}[Nt^{pn}_e(\rho^n_{mt}+\rho^n_{sp})+Zt^{pp}_e(\rho^p_{mt}+\rho^p_{sp})](\sigma^p+\sigma^A)\ , \tag{9}$$

$$U_f=\tfrac{1}{2}[Nt^{pn}_e(\rho^n_{mt}-\rho^n_{sp})+Zt^{pp}_e(\rho^p_{mt}-\rho^p_{sp})](\sigma^p-\sigma^A)\ . \tag{10}$$

We expect U_e and U_f to be of comparable size, with U_f vanishing only if $\rho^n_{mt}=\rho^n_{sp}$ *and* $\rho^p_{mt}=\rho^p_{sp}$, an equality we do not expect to be true [see Eq. (18) and (20)]. The importance of the f term can be determined phenomenologically by measuring how much some of the tensor polarization observables differ (see Sec. II C).

In our optimal, impulse approximation,[5,6] the first-order optical potential $U^{(1)}$—which should be a convolution of t^{NN} over nuclear functions—is factored into the form (1). Since t^{NN} is not a rapidly varying function of energy at intermediate energies, we expect this to be a good approximation. The choice of the initial target-nucleon momentum

$$\mathbf{p}_0=-\frac{\mathbf{k}}{\mathbf{A}}+\frac{A-1}{2A}\mathbf{q} \tag{11}$$

optimizes the factorization approximation and also means there is a different optimal momentum and NN energy for each p-nucleus scattering angle. The NN T matrices in (1) are functions of the initial and final projectile- and target-nucleon momenta, for example,

$$t^{pn}_e=\langle\mathbf{k}',\mathbf{p}_0-\mathbf{q}|t^{pn}_e(\omega)|\mathbf{k},\mathbf{p}_0\rangle\ . \tag{12}$$

In these calculations we choose ω, the NN subenergy in the NN COM, as the "three-body energy" ω_{3B}, that is, we view the nucleus as an active nucleon of momentum $\mathbf{p}_0$ plus a passive core of momentum $\mathbf{P}$. The NN energy ω_{3B} is then the projectile-nucleus total energy decreased by that of the passive core. In terms of four-momenta we take

$$\omega^2_{3B}=(k^\mu_p+k^\mu_A-P^\mu)^2\ , \tag{13}$$

$$P^2\simeq\left[\frac{A-1}{A}\right]\left[k^2+\frac{q^2}{4p^2_F}+\mathbf{q}\cdot\mathbf{k}\right]\ , \tag{14}$$

where the Fermi momentum p_F, is chosen as 185 MeV/c.

The off-shell NN t matrix in the p-^{3}He COM is related to the t in the NN COM via

$$\langle\mathbf{k}',\mathbf{p}'|t(\omega)|\mathbf{k},\mathbf{p}\rangle=\gamma_{LPT}\langle\boldsymbol{\kappa}'|\tilde{t}(\omega)|\mathbf{k}\rangle \tag{15}$$

$$\gamma_{LPT}=\left[\frac{E_p(\kappa)E_p(\kappa')E_n(\kappa)E_n(\kappa')}{E_p(k)E_p(k')E_n(p)E_n(p')}\right]^{1/2}\ , \tag{16}$$

where γ_{LPT} arises from conservation of probability. $\boldsymbol{\kappa}$ and $\boldsymbol{\kappa}'$ are the initial and final NN COM momenta, and are related to $\mathbf{k}$, $\mathbf{k}'$, $\mathbf{p}_0$, and $\mathbf{q}$ via the "angle transformation" (a unique prescription if covariance is demanded in an on-mass-shell theory). Although we do not give de-

tails here, the off-shell kinematics incorporated into our theory critically affects the predictions beyond the small-angle region and is one reason we calculate in momentum space.

The off-shell variation of the NN T matrices in each eigenchannel $\alpha=(JlS)$ is described with a separable potential

$$\langle\kappa'|\tilde{t}_\alpha[\omega(\kappa_0)]|\kappa'\rangle=\frac{g_\alpha(\kappa')g_\alpha(\kappa)}{g_\alpha^2(\kappa_0)}\langle\kappa_0|\tilde{t}_\alpha[\omega(\kappa_0)]|\kappa_0\rangle\ , \quad (17)$$

where $\langle\kappa_0|\tilde{t}_\alpha[\omega(\kappa_0)]|\kappa_0\rangle$ is the on-shell amplitude and $g_\alpha(\kappa)$ is the separable potential's form factor. For the off-shell extrapolation in (17) we use the Graz potential[10] (it closely approximates the on-shell and half-off-shell behavior of the Paris potential). This provides us with the physically motivated (unitary) off-shell behavior arising from finite-range NN forces—as well as the consistency of having comparable relativistic propagators in the two- and many-body problems.

The on-shell NN amplitudes are determined from the phase-shift analyses of Arndt[9] and Saclay[8] (see Ref. 5 for a demonstration of the NN phase shift sensitivity). Since these amplitudes are antisymmetrized, our optical potential inherently includes the exchange of the projectile and struck nucleon—but not antisymmetrization with the unstruck nucleon (the latter being the type included in resonating group calculations). The inclusion of those exchange effects may improve the validity of our model at back angles.

In summary, our basic NN amplitudes are valid for $(10\le T_p\le 750)$ MeV and all scattering angles, contain the full structure of spin $\frac{1}{2}\times\frac{1}{2}$ scattering, independent behavior of the momenta and energy variables, back-angle structure characteristic of exchange (antisymmetry), off-shell behavior based on meson exchanges, a covariant mapping into the p-nucleus reference frame, and on-shell behavior agreeing with recent NN experiments.

B. Nuclear form factors

The optical potential (1) requires four form factors describing the distributions of spin (sp) and matter (mt) for point protons and neutrons. To extract these $\rho(q)$'s from the charge (ch) and magnetic (m) form factors for trinucleons requires the removal of the finite nucleon size and meson-exchange current contributions to $F_{\rm ch}$ and F_m. Finite nucleon size is presumably included in the pN T matrices we use, and the meson currents that couple to a scattered electron would be inappropriate for a scattered proton (we include no such higher-order effects here). The appropriate hadronic form factors are related to the electromagnetic ones by[5]

$$\rho^p_{\rm mt}(q)=F_{\rm ch}(^3{\rm He})/f^p_{\rm ch},\quad \rho^n_{\rm mt}(q)=F_{\rm ch}(^3H)/f^p_{\rm ch}\ , \quad (18)$$

$$\rho^n_{\rm sp}(q)=[\mu_p^2F_m(^3{\rm H})-\mu_n^2F_m(^3{\rm He})]/[f^p_{\rm ch}(\mu_p^2-\mu_n^2)]\ , \quad (19)$$

$$\rho^p_{\rm sp}(q)=\mu_p\mu_n[F_m(^3{\rm H})-F_m(^3{\rm He})]/[2f^p_{\rm ch}(\mu_p^2-\mu_n^2)]\ , \quad (20)$$

where $f^p_{\rm ch}$ is the elementary proton's charge form factor (the dipole fit), and $\mu_{p,n}$ are the nucleon's magnetic moments. Our normalization is

$$\rho^p_{\rm mt}(0)=\rho^n_{\rm mt}(0)=\rho^n_{\rm sp}(0)=1,\ \rho^p_{\rm sp}(0)=0\ . \quad (21)$$

For the f's we use the pure nucleonic part of the form factors from the three-body calculations of Hadjimichael *et al.*;[12] these reproduce the electron scattering data out to $\sim 80\ {\rm fm}^{-2}$.

TABLE I. X_{0000}: Differential cross section (unpolarized PTP'T).

No.	Name	Equation
1	$\sigma=I_{0000}$	$(\lvert a\rvert^2+\lvert b\rvert^2+\lvert c\rvert^2+\lvert d\rvert^2+\lvert e\rvert^2+\lvert f\rvert^2)/2$

C. Polarization observables

As discussed by Bystricky, Lehar, and Winternitz[3] for the NN case, and LaFrance and Winternitz[4] for nonidentical particles, there are some 36 possible spin observables for p-^{3}He scattering. Since we do not find a simple enumeration of the observables illuminating, we instead classify them according to the degree of difficulty encountered in their measurement (the number of initial and final polarizations required). The different classes are enumerated in Tables I–VII.

The notation follows that of Refs. 3 and 4—with a correction for variable No. 19 $M_{\rm moln}$ given by Ray *et al.*[13] We refer the reader to these references for explanations. The common usage is to call σ a cross section, P a polarization, A an asymmetry, C a polarization correlation, K a polarization transfer, D a depolarization or polarization rotation, and M a scattering matrix. Often we find it clearer to use the tensor notation $X_{P'T'PT}$ with P and T referring to the polarization of the projectile and target in the initial state, P' and T' to the polarization in the final state, and a zero "0" denoting an unpolarized state or an unobserved polarization. The specific directions of the polarizations are given by the letters n, m, and l, and refer to the vectors of Eq. (3) and Fig. 1: n "normal," m along "momentum transfer," and l "longitudinal" or "sideways." (And then to avoid all those subscripts we give each observable a number.)

Table I lists the single, experimental observable σ, the differential cross section, which can be measured with an initially unpolarized projectile and target, and without observation of the polarizations in the final state. In the third column is the relation of the observable to the various p-^{3}He, amplitudes of (6) (we discuss our calculation of it and give sample results in the following).

Table II lists the possible observables when only one component of the polarization tensor is nonzero, and their relations to the spin amplitudes of (6). We see (ob-

TABLE II. $X_{P'000}$: One-component Polarization Tensor (polarized projectile').

No.	Name	Equation	Vary
2	$P^{(1)}=P_{n000}=A_{00n0}$	$\mathrm{Re}(a^*e+b^*f)/\sigma$	Y
2'	$P^{(2)}=P_{0n00}=A_{000n}$	$\mathrm{Re}(a^*e-b^*f)/\sigma$	Y

TABLE III. $X_{P'0P0}$: Two-component polarization tensor (polarized projectile, unpolarized target, polarized projectile'). The asterisk indicates a repeated observable.

No.	Name	Equation	Vary
3	D_{n0n0}	$(\|a\|^2+\|b\|^2-\|c\|^2-\|d\|^2+\|e\|^2+\|f\|^2)/2\sigma$	Y
4	$D_{l0m0}=-D_{m0l0}$	$\mathrm{Im}(b^*e+a^*f)/\sigma$	Y
5	D_{m0m0}	$\mathrm{Re}(a^*b+c^*d-e^*f)/\sigma$	Y
5′	D_{0m0m}	$\mathrm{Re}(a^*b+c^*d+e^*f)/\sigma$	Y
6	D_{l0l0}	$\mathrm{Re}(a^*b-c^*d-e^*f)/\sigma$	Y
2	A^*_{00n0}	$\mathrm{Re}(a^*e+b^*f)/\sigma$	Y

servable No. 2) that symmetry[3] requires P_{n000}, the polarization of the scattered projectile in a direction normal to the scattering plane for an unpolarized beam and target, to equal A_{00n0}, the right-left asymmetry of the scattered particle when a beam polarized in the $\hat{n}$ direction scatters from an unpolarized target.

The fourth column of Table II (and of subsequent tables) indicates the observable's "sensitivity" or degree of variability, that is, whether we expect it to have a large variation in the forward hemisphere. We limit this rating to the forward hemisphere, since for larger angles the cross section are so small that even though the spin observable may be large (they are the ratio of cross sections), the counting rate (and reliability of the theory after sustaining cancellations producing a drop of several orders of magnitude) is low. We deduce this sensitivity or variability by observing that the a, b, and e amplitudes are dominant for p-^{3}He, and that the cross section σ (observable No. 1) contains the "large" sum $|a|^2+|b|^2+|e|^2$. Thus for a spin observable to have high variation it must contain the product of two large amplitudes—as does the cross section—so division by the large σ will not produce a small number. For example, variable No. 4 D_{l0m0} contains b^*e and is large, but No. 8 K_{l00m} contains c^*e and is small.

Starting with Table II, we give primed and unprimed versions of those spin observables which differ from each other only by the sign with which the f term enters; if the projectile and target were identical, these observables would be equal. For example, variable No. 2′, P_{0n00}, the polarization of the recoiling target particle, differs from observable No. 2, the polarization of the scattered projectile. As we shall see, the calculated primed and unprimed observables differ most when f is mixed with a large amplitude like a, b, or c. Yet if this were the case, these observables would have a high variation, and so the Y in the last column of the tables also indicates if the primed and unprimed variables differ significantly.

Table III lists the five observables accessible when two components of the polarization tensor corresponding to a polarized projectile (P) and a polarized scattered projectile (P') are nonzero (we consider determination of the target's final polarization an impractically difficult measurement). Again we see that some observables are predicted to be more sensitive than others; e.g., since variables No. 5 and No. 6 differ only by the sign of the small c^*d term, their variation should be similar. In other words, the depolarization in the momentum transfer $\hat{m}$ direction is similar to the depolarization in the longitudinal $\hat{l}$ direction (indeed both are in the scattering plane)—yet significantly different from variable No. 3, the depolarization of a spin normal to the scattering plane.

Table IV lists five additional observables corresponding to two nonzero components of the polarization tensor (T and P'). Observable No. 7, the polarization transferred along the normal direction, is predicted to be sensitive. The polarization transfers within the plane, No. 8 and No. 8′ are predicted to be similar to each other since d is small.

Table V lists five observables accessible when the P and T components of the polarization tensor are nonzero. Observable No. 11, the asymmetry when P and T are in the normal direction, is predicted to vary highly, while No. 12 and No. 12′ are predicted to be similar (c is small).

Table VI lists 13 additional observables accessible when three components of the polarization tensor (P,T,P') are nonzero. We see that five of them are predicted to be sensitive.

Finally, in Table VII we give the four observables re-

TABLE IV. $X_{P'00T}$: Two-component polarization tensor, unpolarized projectile, polarized target, polarized projectile'.

No.	Name	Equation	Vary
7	K_{n00n}	$(\|a\|^2-\|b\|^2+\|c\|^2-\|d\|^2+\|e\|^2-\|f\|^2)/2\sigma$	0
8	K_{l00m}	$\mathrm{Im}(c^*e+d^*f)/\sigma$	N
8′	K_{0lm0}	$\mathrm{Im}(c^*e-d^*f)/\sigma$	N
9	K_{m00m}	$\mathrm{Re}(a^*c+b^*d)/\sigma$	N
10	K_{l00l}	$\mathrm{Re}(a^*c-b^*d)/\sigma$	N
2	A^*_{000n}	$\mathrm{Re}(a^*e-b^*f)/\sigma$	Y

TABLE V. X_{00PT}: Two-component polarization tensor (polarized projectile, polarized target, no polarized projectile').

No.	Name	Equation	Vary
11	A_{00nn}	$\frac{1}{2}(\|a\|^2-\|b\|^2-\|c\|^2+\|d\|^2+\|e\|^2-\|f\|^2)/\sigma$	Y
12	A_{00lm}	$-\mathrm{Im}(d^*e+c^*f)/\sigma$	N
12'	A_{00ml}	$-\mathrm{Im}(d^*e-c^*f)/\sigma$	N
13	A_{00mm}	$\mathrm{Re}(a^*d+b^*c)/\sigma$	N
14	A_{00ll}	$-\mathrm{Re}(a^*d-b^*c)/\sigma$	N

quiring all components of the polarization tensor—what we consider impractically difficult measurements.

III. COMPUTATION OF POLARIZATION OBSERVABLES

We use the optical potential (1) with its (central, spin-orbit, and tensor forces) spin dependences to calculate the p-^{3}He spin observables. We first make a numerical, angular momentum decomposition[6] and then solve the coupled partial-wave Lippmann-Schwinger equations

$$T^{JS}_{ll'}(k',k)=U^{JS}_{ll'}(k',k) + \frac{2}{\pi}\sum_L \int_0^\infty p^2 dp \frac{U^{JS}_{lL}(k',p)T^{JS}_{Ll'}(p,k)}{E(k_0)-E(p)+i\epsilon} . \quad (22)$$

Here k_0 is the magnitude of the on-energy-shell momentum, relativistic energies are used in the denominator, and the sum is over L the orbital angular values coupled for a fixed total angular momentum J value. The Coulomb potential is not included.

The proper inclusion of U_f, the f-like term in the optical potential, requires coupling the singlet and triplet amplitudes $T^{J0}_{ll'}$ and $T^{J1}_{ll'}$ in (22). As a first step in that complicated restructuring, we include U_f's contribution in Born or "impulse" approximation; that is, we take the f term of the p ^{3}He amplitude (6) to be

$$f^A(\theta)\simeq \mathcal{N}U_f(\mathbf{k}',\mathbf{k};E) \quad (23)$$

(A refers to the amplitude for the nucleus). We determine the normalization factor $\mathcal{N}$ by requiring the ratio f^A/e^A in the forward direction to be the same as that of the potential which generated them

$$\frac{f^A(0°)}{e^A(0°)}=\frac{U_f(0°)}{U_e(0°)} \Rightarrow \mathcal{N}=\frac{e^A(0°)}{U_e(0°)} . \quad (24)$$

This ratio is approximately $\frac{1}{3}-\frac{1}{6}$ for p ^{3}He (and smaller for p ^{12}C).

As detailed in Refs. 6 and 5, we use the $T^{JS}_{ll'}(k_0,k_0)$'s to construct the Stapp amplitudes for p-^{3}He scattering, and from these generate the a,b,c,d,e,f amplitudes of Eq. (6) at each scattering angle. With $a-f$ normalized according to the conventions of Refs. 3 and 4, we follow their prescription to convert the complex $a-f$'s into all of the possible spin observables.

The results of our calculations are displayed in Figs. 2–4. In Fig. 2 we see the differential cross section, variable No. 1, for energies from 250 to 650 MeV with no Coulomb effects included. The oscillations present at 250 MeV subside at higher energies, a consequence we suspect of the improved validity of the impulse approximation at 300 MeV and above. While these cross sections look quite smooth on this seven-decade semilog

TABLE VI. $X_{P'0PT}$: Three-component tensor, polarized projectile, polarized target, polarized projectile'.

No.	Name	Equation	Vary
15	$M_{l0ln}=M_{m0mn}$	$\mathrm{Re}(b^*e-a^*f)/\sigma$	Y
15'	N_{0lnl}	$\mathrm{Re}(b^*e+a^*f)/\sigma$	Y
16	M_{l0nl}	$\mathrm{Re}(c^*e-d^*f)/\sigma$	N
16'	M_{m0nm}	$\mathrm{Re}(c^*e+d^*f)/\sigma$	N
17	M_{n0ll}	$-\mathrm{Re}(d^*e-c^*f)/\sigma$	N
17'	N_{0nll}	$-\mathrm{Re}(d^*e+c^*f)/\sigma$	N
18	M_{l0mn}	$-\mathrm{Im}(a^*b+c^*d-e^*f)/\sigma$	Y
18'	N_{0lnm}	$-\mathrm{Im}(a^*b+c^*d+e^*f)/\sigma$	Y
19	M_{m0ln}	$\mathrm{Im}(a^*b-c^*d-e^*f)/\sigma$	Y
20	M_{l0nm}	$-\mathrm{Im}(a^*c+b^*d)/\sigma$	N
21	M_{m0nl}	$\mathrm{Im}(a^*c-b^*d)/\sigma$	N
22	M_{n0lm}	$\mathrm{Im}(a^*d+b^*c)/\sigma$	N
23	M_{n0ml}	$\mathrm{Im}(a^*d-b^*c)/\sigma$	N
2'	M^*_{n0nn}	$\mathrm{Re}(a^*e-b^*f)/\sigma$	Y

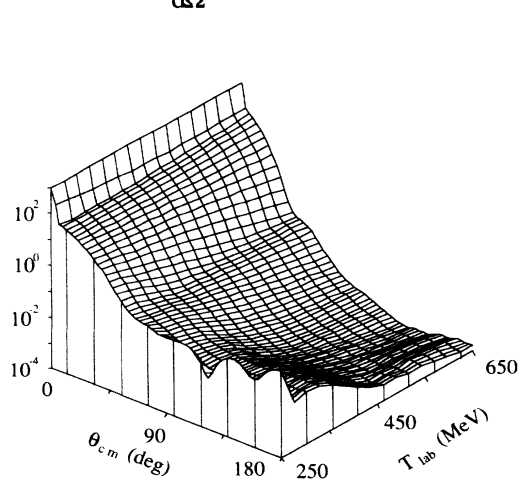

FIG. 2. The p-^{3}He differential cross section as a function of both the COM scattering angle between 0 and 180°, and of the lab kinetic energies between 250 and 650 MeV.

TABLE VII. $X_{P'T'PT}$: Four-component tensor (all states polarized).

No.	Name	Equation	Vary
24	C_{llll}	$(+\|a\|^2+\|b\|^2+\|c\|^2+\|d\|^2-\|e\|^2-\|f\|^2)/2\sigma$	Y
24″	C_{llmm}	$(-\|a\|^2+\|b\|^2+\|c\|^2-\|d\|^2+\|e\|^2-\|f\|^2)/2\sigma$	Y
25	C_{lllm}	$\mathrm{Im}(a^*e-b^*f)/\sigma$	Y
25′	C_{llml}	$\mathrm{Im}(a^*e+b^*f)/\sigma$	Y

scale, the forward diffractive peak is evident at the higher energies; if the nucleus were larger in size (like carbon), the diffraction would be greater. Also evident in Fig. 1 are structures (rises) in the back-angle scattering arising from the antisymmetrized NN amplitudes and the transformations between the pN and p-nucleus COM frames.

In Fig. 3 we compare predictions for the p-^{3}He analyzing power A_{00n0}, variable No. 2, at 415 MeV with the data of Hassel *et al.*[14] Physically, the pronounced variations near 50 and 100 degrees arise from slight displacements in angle of the cross sections for scattering to the right and left. The improved agreement with experiment when the f amplitude is included is evident, as is the apparent loss of validity of the theory at the largest angles.

In Fig. 4 we present in three-dimensional form our main results, the predicted angle and energy dependences of spin observables. The variation is generally quite smooth as a function of either energy or angle—except for the ripples at large angles and high energies which indicate to us a breakdown of our theoretical or numerical formulation.

Some immediate understanding of these visualizations is obtained by examining the "variability" column of Tables II–VII. The checked variables with a Y in the last column generally have a higher variation at small angles than the N variables, and the primed and unprimed variables differ much only if they show a Y in the last column (in fact to avoid near duplication, we refrain from showing most of the N-primed variables).

More detailed examinations of all figures indicate the following:

(1) The large difference between D_{n0n0} (No. 3) and K_{n00n} (No. 7), that is, between Figs. 4(c) and 4(h), confirms that the p-^{3}He b amplitude is large.

(2) The small difference between D_{m0m0} (No. 5) and D_{l0l0} (No. 6), that is, between Figs. 4(e) and 4(g), confirms that the p-^{3}He c and d amplitudes are small, also confirmed by the small difference between K_{n0n0} (No. 7) and A_{00nn} (No. 11), that is, between Figs. 4(h) and 4(m).

(3) The large difference between D_{m0m0} (No. 5) and D_{0m0m} (No. 5′), that is, between Figs. 4(e) and 4(f), confirm that the p-^{3}He f amplitude is big.

(4) The small difference between K_{l00n} (No. 8) and K_{0lm0} (No. 8′), that is, between Figs. 4(i) and 4(j), confirms that the p-^{3}He d amplitude is small—in which case a primed and unprimed observable differ slightly.

(5) All polarization observables show a sensitivity to nuclear structure effects (exclusion of meson-exchange currents from the form factors), and to NN amplitudes (differences between Arndt[9] or Saclay[8] phases) equivalent to that found in Ref. 5.

A poignant question after looking at all these figures and observables may well be "what can they teach us?" Phenomenologically they determine the complex a–f amplitudes for the p-^{3}He system at each energy, a determination which is by no means simple. For example, in

TABLE VIII. Selected amplitudes in terms of observables.

Amplitude		Observables
$\|a\|^2$	=	$\sigma[X^3+X^7+X^{24}-X^{24''}]/2$
$\|b\|^2$	=	$\sigma[X^3-X^7+X^{24}+X^{24''}]/2$
$\|c\|^2$	=	$\sigma[1-X^3+X^7-X^{11}]/2$
$\|e\|^2$	=	$\sigma[1+X^{11}-X^{24}+X^{24''}]/2$
$\|f\|^2$	=	$\sigma[1-X^{11}-X^{24}-X^{24''}]/2$
a^*b	=	$\sigma[X^5+X^6+i(X^{18}-X^{22})]/2$
a^*c	=	$\sigma[X^9+X^{10}+i(X^{20}-X^{21})]/2$
c^*d	=	$\sigma[X^5-X^6+i(X^{19}+X^{18})]/2$

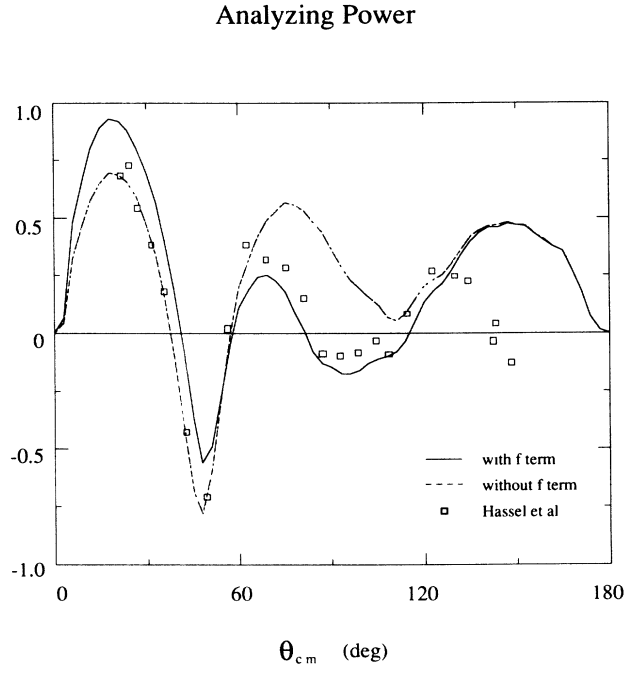

FIG. 3. The analyzing power A_{00n0} at 415 MeV showing the effect of including the p-^{3}He f amplitude (not included in our previous calculations). The data are from Ref. 14.

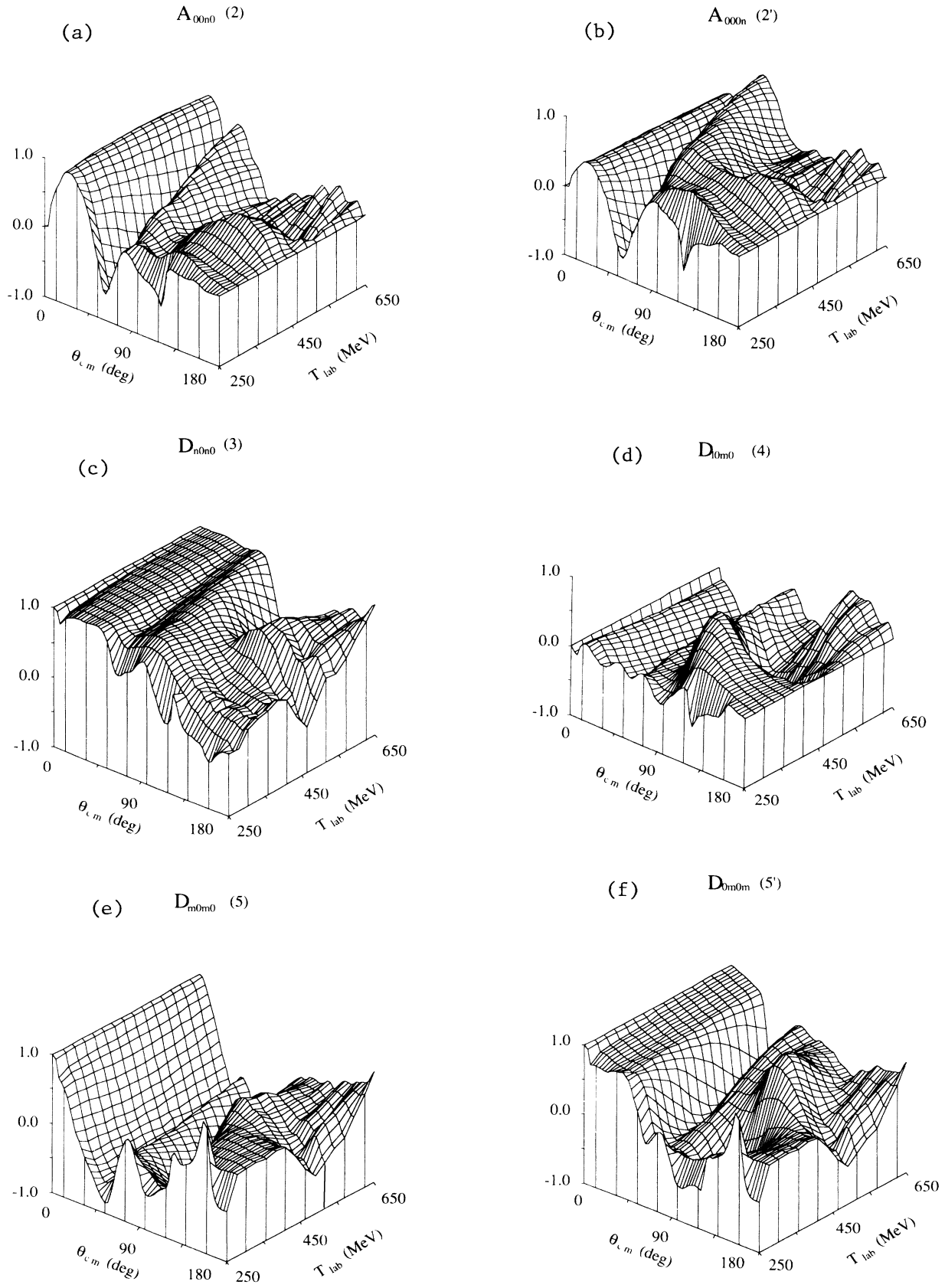

FIG. 4. The p-^{3}He spin observables $X_{P'T'PT}$ (defined in the tables) as a function of both the COM scattering angle between 0 and 180°, and of the lab kinetic energies between 250 and 650 MeV. The primed and unprimed observables differ only by the sign with which the f amplitude enters.

(g) D_{l0l0} (6)

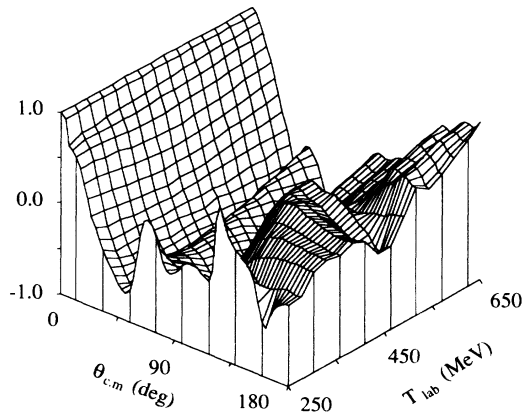

(h) K_{n00n} (7)

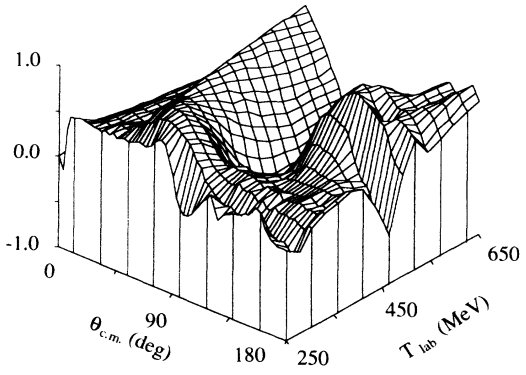

(i) K_{l00m} (8)

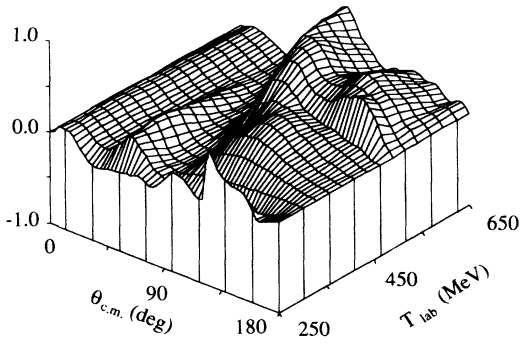

(j) K_{0lm0} (8')

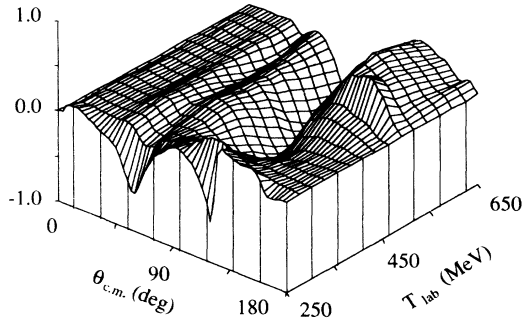

(k) K_{m00m} (9)

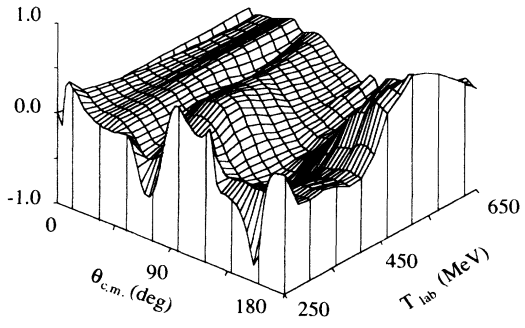

(l) K_{l00l} (10)

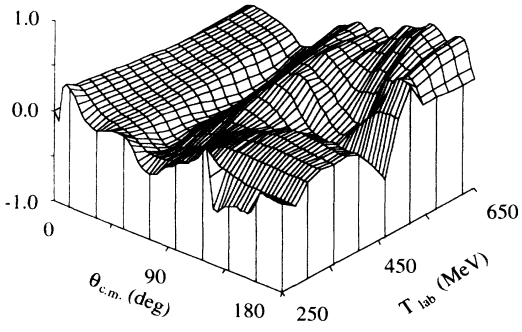

FIG. 4. (*Continued*).

(m) A_{00nn} (11)

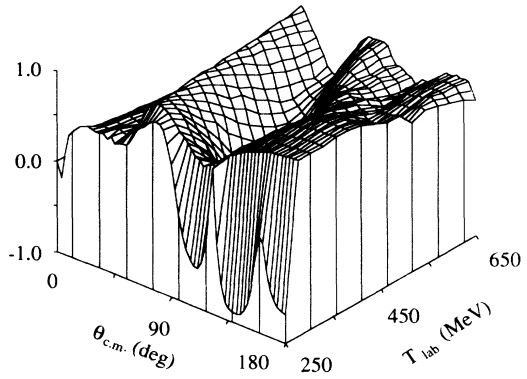

(n) A_{00lm} (12)

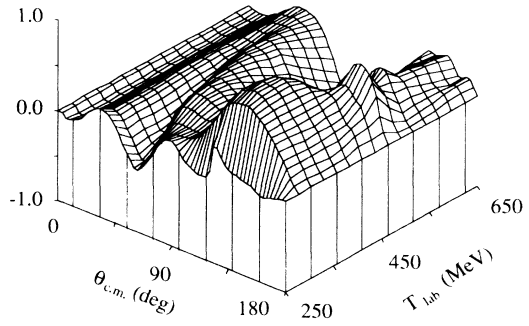

(o) A_{00ml} (12')

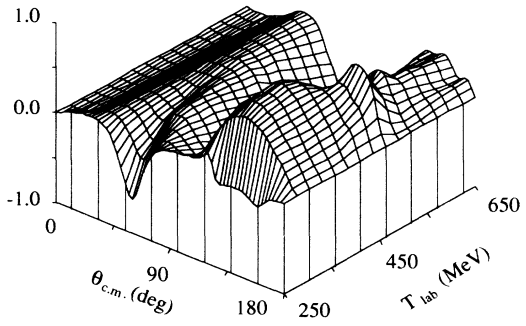

(p) A_{00mm} (13)

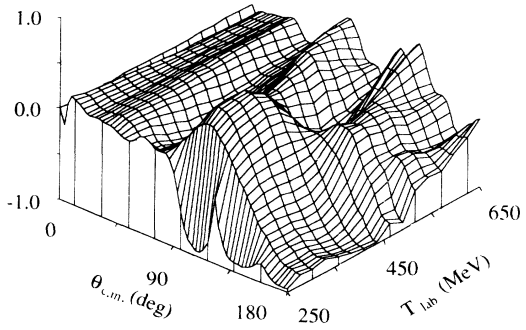

(q) A_{00ll} (14)

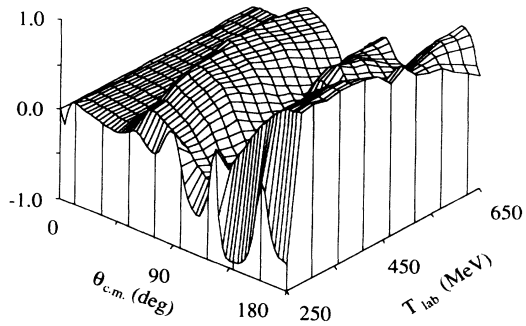

(r) M_{00ln} (15)

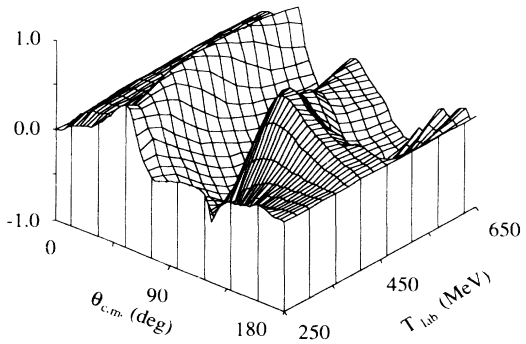

FIG. 4. (*Continued*).

(s) N_{0lnl} (15')

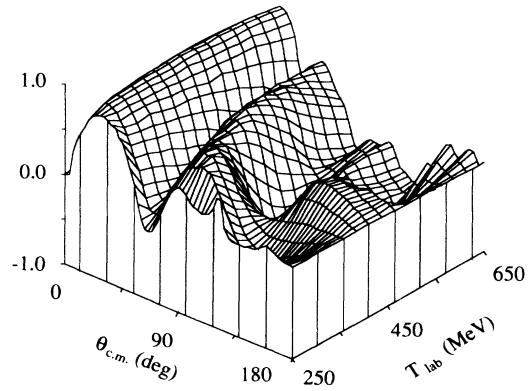

(t) M_{l0nl} (16)

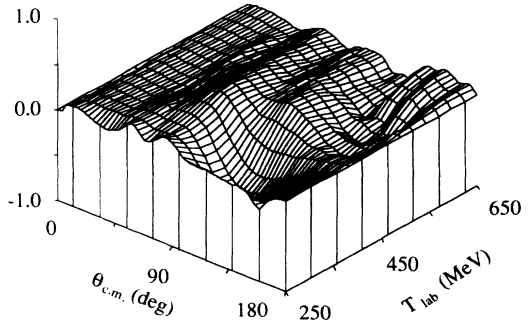

(u) M_{n0ll} (17)

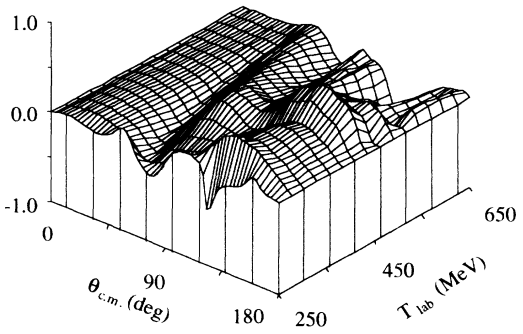

(v) M_{l0mn} (18)

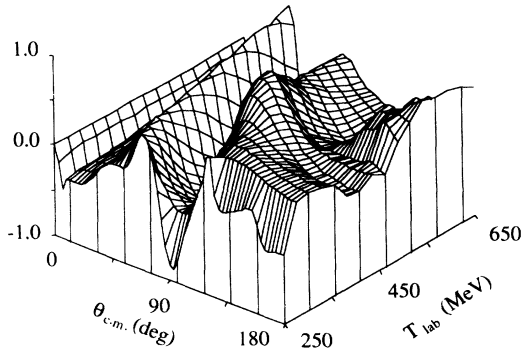

(w) N_{0lnm} (18')

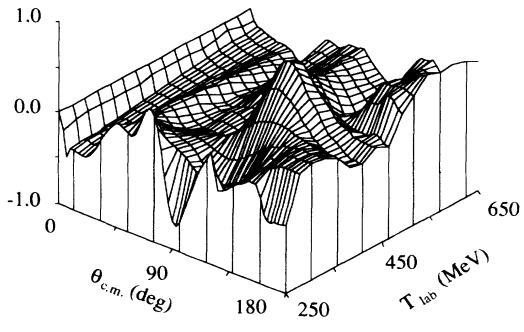

(x) M_{l0nm} (20)

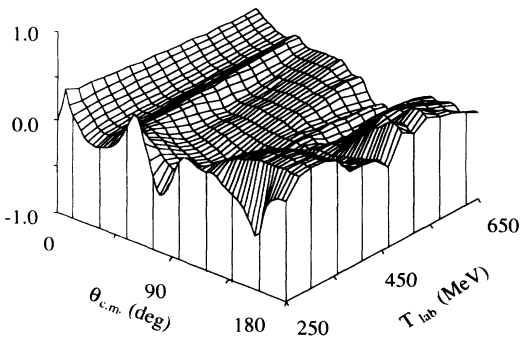

FIG. 4. (*Continued*).

(y) M_{m0nl} (21)

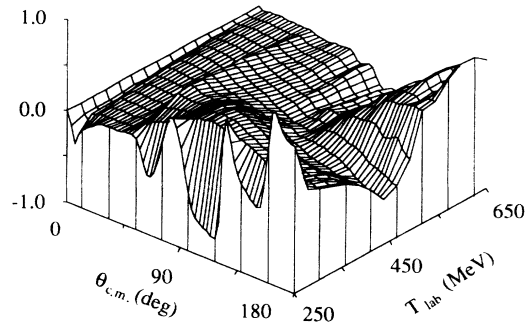

(z) M_{n0lm} (22)

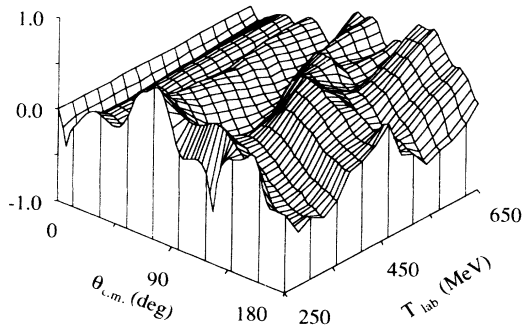

(a') M_{n0ml} (23)

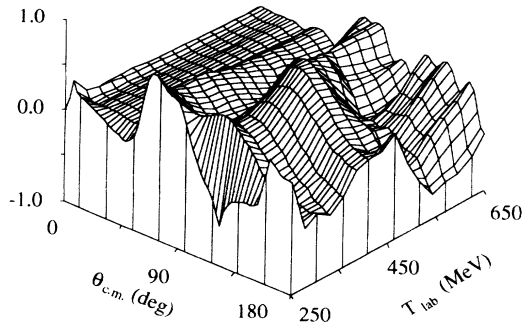

(b') C_{llll} (24)

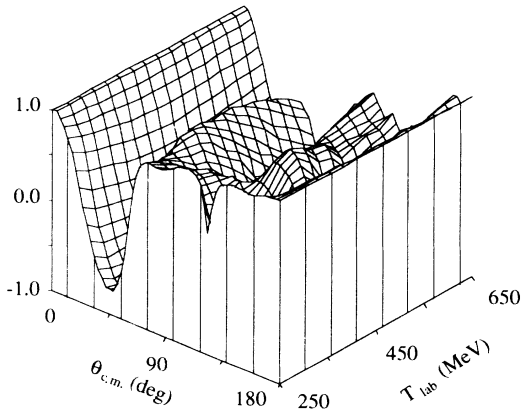

(c') C_{llmm} (24")

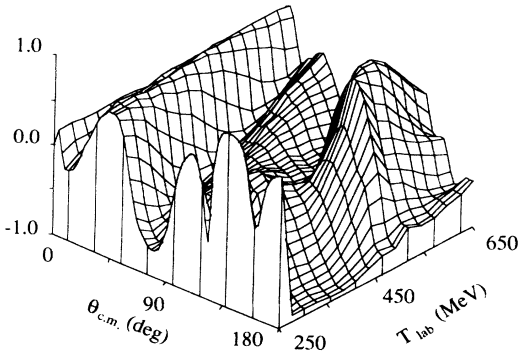

(d') C_{lllm} (25)

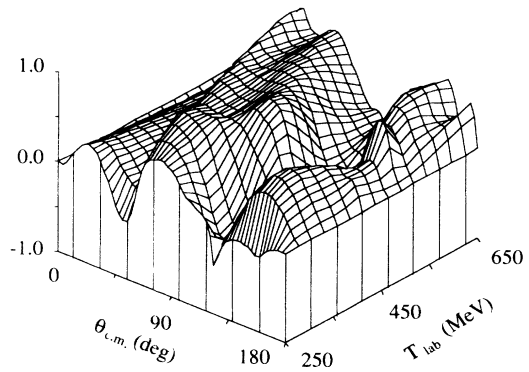

FIG. 4. (*Continued*).

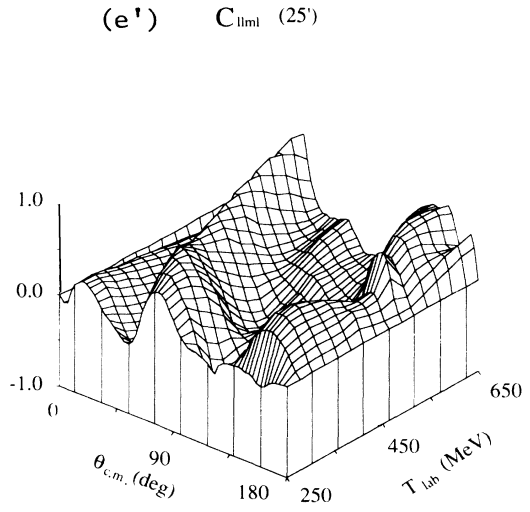

FIG. 4. (*Continued*).

Table VIII we present a reduced version of Table IV of Ref. 3 giving a direct solution for the amplitudes in terms of the polarization observables (using our numbering scheme). It is by no means trivial to determine an individual amplitude (just as it is nontrivial to determine an individual phase shift).

The theoretical-level answer to what we can learn from these observables is a basic one to nuclear physics. While the high sensitivity to nuclear structure and to the nucleon-nucleon interaction is encouraging, there appears no obvious way to disentangle the two (or three if the related relativistic effects are included). This is clearly an open area of research probably requiring one of the alternative and optimal representation of the polarization observables[15] to provide a more transparent connection between polarization observables and the underlying dynamics.

IV. SUMMARY

We have reorganized the observables for spin $\frac{1}{2}\times\frac{1}{2}$ scattering into different classes based on the difficulty of measurement, and have predicted if each observable is "sensitive," that is, highly variable in the forward hemisphere for medium energy protons. We find that few observables require the very difficult measurement of the recoiling target's polarization. We have also constructed a microscopic (impulse approximation), momentum space, optical potential and studied all the spin variables accessible with a polarized proton beam and a polarized ^{3}He target. For most observables we present the energy and angle dependences in three-dimensional plots which should be useful in planning experiments. In this way it should be possible to learn about the spin structure of the ^{3}He nucleus, the importance of meson-exchange and quark currents within the nucleus, as well as test our knowledge of the nucleon-nucleon interactions.

ACKNOWLEDGMENTS

We are pleased to thank Lindsey Birge and Ken Amos for illuminating conversations on polarization observables, Bill Thompson for encouraging us to publish them, and Lanny Ray for his encouragement and diplomatic persistence about those f amplitudes. The warm hospitality of the Physics Department of Melbourne University, and of IBM Watson Research, where some of this paper was written, is also acknowledged and appreciated. This work was supported in part by the U.S. Department of Energy.

[1]J. M. Blatt and V. F. Weisskopf, *Theoretical Nuclear Physics* (Wiley, New York, 1952).

[2]Proceedings of the LAMPF Workshop on Physics with Polarized Nuclear Targets, 1986, edited by G. Burleson, W. Gibbs, G. Hoffmann, J. J. Jarmer, and N. Tanaka (LAMPF Report No. LA-10772-C, 1986).

[3]J. Bystricky, F. Lehar, and P. Winternitz, J. Phys. (Paris) **39**, 1 (1978).

[4]P. La France and P. Winternitz, J. Phys. (Paris) **41**, 1391 (1980)

[5]R. H. Landau and M. Sagen, Phys. Rev. C **33**, 447 (1986); Phys. Lett. **158B**, 197 (1985).

[6]M. J. Paez and R. H. Landau, Phys. Rev. C **29**, 2267 (1984); **30**, 1757 (1984); Phys. Lett. **142B**, 235 (1984).

[7]L. Ray, private communications.

[8]J. Bystricky, C. Lechanoine, and F. Lehar, Saclay Report No. D Ph PE.79-01, 1979.

[9]R. A. Arndt, L. D. Roper, R. A. Bryan, R. B. Clark, B. J. VerWest, and P. Signell, SAID dial up system.

[10]K. Schwarz, J. Haidenbauer, and J. Frohlich, Phys. Rev. C **86**, 456 (1986).

[11]For a spin-saturated ($S=0$) nucleus we have $\langle\sigma_2\rangle=0$, which means there is no independent f term.

[12]E. Hadjimichael, B. Goulard, and R. Bournais, Phys. Rev. C **27**, 831 (1983).

[13]L. Ray, G. W. Hoffmann, M. L. Barlett, J. D. Lunpe, B. C. Clark, S. Hama, and R. L. Mercer, Phys. Rev. C **37**, 1169

(1988).
[14]D. K. Hassell, A. Bracco, H. P. Gubler, W. P. Lee, W. T. H. van Oers, R. Abegg, J. M. Cameron, L. G. Greeniaus, D. A. Hutcheon, C. A. Miller, G. A. Moss, G. Roy, M. B. Epstein, D. J. Margaziotos, A. W. Stetz, and H. Postma, Phys. Rev. C **34**, 236 (1986).
[16]G. R. Goldstein and M. J. Moravscik, Phys. Lett. **157B**, 235 (1985); Phys. Res. **227**, 108 (1984).